

# N-electron valence state perturbation theory based on density matrix renormalization group reference functions, with applications to chromium dimer and photovoltaic polymers

Sheng Guo, Mark A. Watson, Weifeng Hu, Qiming Sun, Garnet Kin-Lic Chan<sup>1</sup>  
*Department of Chemistry, Princeton University, Princeton, New Jersey 08544, USA*

(Dated: 19 October 2015)

The second order n-electron valence state perturbation theory (NEVPT2) is a relatively cheap way to deal dynamic correlation without intruder state problem or level shift, while density matrix renormalization group (DMRG) is able to deal static correlation with a large active space and to provide reference wave functions needed in multireference perturbation theories. We present a method to combine DMRG and NEVPT2 (DMRG-NEVPT2) through the a general algorithm to compute high order reduced density matrices for DMRG wave function. The capacity of DMRG-NEVPT is demonstrated for calculations of chromium dimer potential energy curve and excited states energy of poly(p-phenylene vinylene).

## I. INTRODUCTION

The density matrix renormalization group (DMRG)<sup>1,2</sup> has made it accessible to employ large active spaces for electronic structure problems in quantum chemistry. Nowadays, it has become quite straightforward to use DMRG as a robust numerical solver for static electron correlation problems. Examples are benchmark solutions of small molecules<sup>3</sup>, transition metal clusters<sup>4,5</sup>, also molecular crystals<sup>6</sup>.

In chemical systems, electron interaction across large energy scales brings many other important chemistry, such as low-lying excited states in conjugated polymers, high-spin ground state in transition metals complexes. Qualitative and quantitative characterizations of these systems generally require correlating many electrons within a large number of orbitals. Direct treatment of such problem is generally impossible, but indirect methodology can apply, for example, by expanding the electron correlation outside active spaces. So far, there are methods which follow with this strategy with using large active spaces, for example, to apply perturbation theory to a large active space, or perform canonical transformation to get an effective Hamiltonian. The DMRG method has been embedded with the second-order perturbation theory<sup>7,8</sup>, complete active space perturbation theory (CASPT), and canonical transformation(CT)<sup>9</sup>, etc., to be extended for dynamic correlation. In these methods, high order reduced density matrices are generally needed, which are theoretically straightforward yet computationally non-trivial to compute.

In this work, we developed a general way to compute high order reduced density matrix (RDM) for DMRG wave functions. On the top of RDM calculations, we implemented the second order  $n$ -electron valence state perturbation theory (NEVPT2)<sup>10–12</sup>, an intruder-state-free multireference perturbation theory, with DMRG reference wavefunctions, called DMRG-NEVPT2. Then we applied it to study potential energy curve of chromium dimer and excitation energies of the quasi-one dimen-

sional photovoltaic molecule poly(p-phenylene vinylene) (PPV). The calculations for the potential energy curve of chromium dimer is one of the most notorious and demanding problem in ab-initio quantum chemistry. This system has been widely studied by many methods<sup>7,13–19</sup>. It is good system to demonstrate the capacity of DMRG-NEVPT2. PPV has always been of great interest by photophysists and photochemists, as it is well known for its charge-transfer properties upon photoexcitations<sup>20,21</sup>. The first optically bright state  $1^1B_u$  whose polaronic feature is suggested to be responsible for the charge-transfer behavior, is estimated to lie below the  $2^1A_g$  with a small gap of 0.7eV<sup>22</sup>. Many theoretical studies of PPV are based on model Hamiltonian, such as Pariser–Parr–Pople (PPP) model,<sup>23,24</sup> or semi-empirical quantum chemistry method<sup>25</sup>. However, ab initio quantum chemistry calculation were hardly reported due to the unaffordable computations to including the dynamic correlation and static correlation at the same time for such a system with many  $\pi$  orbitals, which need to be considered as active space in complete active space (CAS) calculations. With DMRG-NEVPT2, now it is possible to compute the excitation energies and energy orders of different states accurately.

### A. N-electron valence state perturbation theory

In this section, we briefly review the strongly contracted NEVPT2<sup>11,12</sup>, a second-order multireference perturbation theory. The target zero-order wave function is defined as

$$P_{CAS} H P_{CAS} |\Psi_m^{(0)}\rangle = E_m^{(0)} |\Psi_m^{(0)}\rangle \quad (1)$$

with  $P_{CAS} = \sum_{I \in S} |I\rangle \langle I|$  is the projector onto the CAS space.

The zero order Hamiltonian is chosen in the form give by Dyall<sup>26</sup>:

$$H^D = H_i + H_v + C \quad (2)$$

where  $H_i$  is a one-electron (diagonal) operator in non-active subspace:

$$H_i = \sum_{i,\sigma}^{core} \epsilon_i \hat{a}_{i,\sigma}^\dagger \hat{a}_{i,\sigma} + \sum_{r,\sigma}^{virt} \epsilon_r \hat{a}_{r,\sigma}^\dagger \hat{a}_{r,\sigma} \quad (3)$$

where  $\epsilon_i$  and  $\epsilon_r$  are orbital energies.

$H_v$  is a two-electron operator confined to the active space:

$$H_v = \sum_{ab,\sigma}^{act} h_{ab}^{eff} \hat{a}_{a,\sigma}^\dagger \hat{a}_{b,\sigma} + \sum_{abcd,\sigma_1,\eta}^{act} \langle ab|cd \rangle \hat{a}_{a,\sigma}^\dagger \hat{a}_{b,\eta}^\dagger \hat{a}_{d,\eta} \hat{a}_{c,\sigma} \quad (4)$$

where  $h_{ab}^{eff} = h_{ab} + \sum_i^{core} (2 \langle ai|bi \rangle - \langle ai|ib \rangle)$

and  $C$  is a constant to ensure that  $H^D$  is equivalent to the full Hamiltonian within the CAS space.

The zero order wave functions external to the CAS space, referred to as the “perturbors”, belong to CAS-CI spaces with well defined patterns of the inactive (core+virtual) orbitals and with a given number of active electrons. The perturber functions are written as  $|\Psi_{l,\mu}^{(k)}\rangle$  and the corresponding CAS-CI spaces as  $S_l^{(k)}$ , where  $k$  is the number of electrons promoted to ( $k > 0$ ) or removed from ( $k < 0$ ) the active space,  $l$  denotes the pattern of inactive orbitals and  $\mu$  numerates the various perturbors.

In strongly contracted NEVPT2, utilizes just one function from each  $S_l^{(k)}$  subspace,  $|\Psi_l^{(k)}\rangle = S_l^{(k)} H |\Psi_m^{(0)}\rangle$  with energy given by

$$E_l^{(k)} = \frac{\langle \Psi_l^{(k)} | H^D | \Psi_l^{(k)} \rangle}{\langle \Psi_l^{(k)} | \Psi_l^{(k)} \rangle} \quad (5)$$

And the zero order Hamiltonian becomes

$$H_0 = |\Psi_l^{(k)'}\rangle E_l^{(k)} \langle \Psi_l^{(k)'}| + |\Psi_m^{(0)}\rangle E_m^{(0)} \langle \Psi_m^{(0)}| \quad (6)$$

where  $|\Psi_l^{(k)'}\rangle$  is normalized  $|\Psi_l^{(k)}\rangle$

The bottle neck is the evaluation of energies of perturbors, where up to forth order RDM is needed. 4-RDM is contracted with double electron integral in active space to form auxiliary matrices.<sup>12</sup> In our implementation for DMRG-NEVPT2, 4-RDM is computed on the fly, avoiding storing huge 4-RDM.

Like Kurashige and Yanai’s implementation of DMRG-CASPT2<sup>7</sup>, these auxiliary matrices can be computed with a scaling similar with that of 3-RDM by make special types of operators, which are the contraction of integral and creation (and annihilation) operators. However, the two-electron Hamiltonian in NEVPT2 is much more complex than the Fork operators (which is diagonal if canonical orbitals used) in CASPT2. Many types of contracted operators would be needed in DMRG frame. It is the very hard to implement and the prefactor is big,

even though the scaling is better. Therefore, We only contracted integral and operators in CASCI-NEVPT2, not in DMRG-NEVPT2.

## B. DMRG wavefunction and optimization algorithm

As with other approximate wavefunction methods in quantum chemistry, DMRG is based on an approximate wavefunction ansatz. It is the matrix product state(MPS). A MPS is a non-linear wavefunction, built from contraction of tensors for each orbital in the basis. Limited by the dimension of tensors, called bond dimension,  $M$ , MPS could only explore a small subspace of Hilbert space. By increasing  $M$ , the MPS ansatz will give full configuration interaction (FCI) results. DMRG is a combination of renormalization and truncation algorithms to find a variational and optimal MPS. In practice, two types of MPS are often used in DMRG calculations: an one-site and a two-site MPS.

The one-site MPS is defined as

$$|\Psi\rangle = \sum_{n_1, n_2, \dots, n_p, \dots, n_k} \mathbf{A}^{n_1} \mathbf{A}^{n_2} \dots \mathbf{A}^{n_p} \dots \mathbf{A}^{n_k} \quad (7)$$

Here,  $n_i$  is the occupancy of orbital  $i$ , one of  $\{|\uparrow\rangle, |\downarrow\rangle, |\uparrow\downarrow\rangle\}$  and  $k$  is the number of orbitals. For a given  $n_i$ ,  $\mathbf{A}^{n_i}$  is  $M \times M$  matrix, except that the first and last ones. For  $\mathbf{A}^{n_1}$  and  $\mathbf{A}^{n_k}$ , their dimensions are  $1 \times M$  and  $M \times 1$  respectively. This ensures that for a given string  $n_1 n_2 \dots n_k$ , a slater determinant, the  $\mathbf{A}^{n_1} \mathbf{A}^{n_2} \dots \mathbf{A}^{n_k}$  yields a scalar, the coefficient of the determinant  $|n_1 n_2 \dots n_k\rangle$

Similarly, the two-site MPS is defined as

$$|\Psi\rangle = \sum_{n_1, n_2, \dots, n_p, \dots, n_k} \mathbf{A}^{n_1} \mathbf{A}^{n_2} \dots \mathbf{A}^{n_p, n_{p+1}} \dots \mathbf{A}^{n_k} \quad (8)$$

In DMRG sweep algorithm,  $\langle \Psi | \hat{H} | \Psi \rangle$  is variational optimized. And only a single tensor ( $\mathbf{A}^{n_i}$  or  $\mathbf{A}^{n_i, n_{i+1}}$  for a two-site MPS) in the MPS is updated during the sweep at site  $i$ . It can be considered as solving eigenvalue problem of an effective Hamiltonian, which is a  $4M^2 \times 4M^2$  matrix. This effective Hamiltonian is usually defined through complimentary operators <sup>acitation</sup>. The cost scaling is  $O(k^2 M^3)$  for this eigenvalue problem for one tensor and is  $O(k^3 M^3)$  for a whole sweep optimization.

Compared to an one-site MPS, a two-site MPS has more variational freedom and is able to change quantum numbers during the sweep. It helps avoid local minimum. However, the two-site MPS has N-representation problem: the converged two-site MPS is still different at different position of sweep. Based on a two-site MPS, expectation values, for example reduced density matrix, which often used to characterize a state and is essential for dynamic correlation calculations, have no unique results. Therefore, the strategy, “two-site to one-site” (a

two-site MPS optimization followed by an one-site one), is widely used.

### C. Reduced density matrix (RDM)

From now on, when we refer MPS, it means an one-site MPS, because it is needed in reduced density matrix and dynamic correlation calculations.

The 2-RDM is defined in this way

$$\gamma_{i,j,k,l} = \sum_{\sigma,\tau} \langle \Psi | a_{i,\sigma}^\dagger a_{j,\tau}^\dagger a_{k,\tau} a_{l,\sigma} | \Psi \rangle \quad (9)$$

It is similar for the higher order reduced density matrix.

It is not affordable to build and store  $k^{2N}$  operators used in N-RDM. And for RDM, the expectation value rather than the operators needed. There is no need to build these complicate operators. One efficient way is to distribute the indices (orbital label)  $i, j, k, l$  among different orbital subspace for different blocks in DMRG.<sup>27,28</sup> The complicate operators are the tensor product of small operators on different blocks. If small operators are contracted with the wave function before doing tensor product. The tensor product will become dot product of operators. It is much cheaper. Below are the details.

Operators like  $\hat{a}_i^\dagger \hat{a}_j^\dagger \dots \hat{a}_m \hat{a}_n \dots$  can be permuted into a form like  $\hat{o}_{i'} \hat{o}_{j'} \dots \hat{o}_{m'} \hat{o}_{n'}$ , with  $i' \leq j' \leq \dots \leq m' \leq n'$  and  $\hat{o}$  is  $\hat{a}$  or  $\hat{a}^\dagger$ . A string with  $N$   $\hat{a}$  and  $N$   $\hat{a}^\dagger$  determines the type of the operator. We call it “type pattern”. Then the string is split into several small pieces according to blocks (orbital subgroups) in DMRG sweep.

There are three blocks in DMRG sweep algorithm. The system block ( $\mathcal{S}$ ) is expanded during the sweep and the operators on it can be easy build on the flying. The dot block ( $\mathcal{D}$ ) is composed of a single site and its operators are extremely simple and cheap. The environment block ( $\mathcal{E}$ ) was computed from  $\mathcal{S}$  in previous sweep in reverse direction, and its operators needed to be precomputed and stored (usually on disk). The  $2N$  orbital labels of  $\hat{O}$  is needed to be partitioned onto the three blocks. It is computational favorable to put more orbital labels on  $\mathcal{D}$  and put few orbital labels on  $\mathcal{E}$ . And the numbers of orbital labels on  $\mathcal{S}$  and  $\mathcal{E}$  need to be balanced, otherwise number of operators on one block will be extremely big. For most RDM element (not for element like  $\gamma_{0,0,0,0}$ ), at least one orbital label could be put on  $\mathcal{D}$  and at most  $N-1$  orbital labels on  $\mathcal{E}$  by change the position of the dot site. The set  $\{n_{\mathcal{S}}, n_{\mathcal{D}}, n_{\mathcal{E}}\}$  determines the numbers of orbital labels on different blocks. It is called “number pattern”. In general, every number pattern is valid if the number of orbital labels on  $\mathcal{S}$  is no more than  $N$ , that on  $\mathcal{D}$  is no more than 4 and that on  $\mathcal{E}$  is no more than  $N-1$ , except the edge cases for the first step and last step in the sweep (in the appendix). And nearly every “type pattern” could be combined with all “number patterns” if with some restrictions (in appendix).

With above process, the types of operators needed on  $\mathcal{S}$ ,  $\mathcal{D}$ , and  $\mathcal{E}$  are determined for each pattern ( “type pattern” and “number pattern”). Loop the orbital labels of operators, we can build all operators we need. There are about  $O(N^k)$  operators, most of which are on  $\mathcal{S}$ . The computation for generate these operators are  $O(k^N M^3)$  for one step at the sweep and are  $O(k^{N+1} M^3)$  in total.

After building operators on each block,  $\hat{O}^S$ ,  $\hat{O}^D$ ,  $\hat{O}^E$ , combine  $\hat{O}^S$  and  $\hat{O}^D$  into  $O^L$ , a big left block  $\mathcal{S} \otimes \mathcal{D}$ . (Combining  $\mathcal{E}$  and  $\mathcal{D}$  only for RDM calculations is also feasible.) The  $\mathcal{E}$  is the right block. RDM element  $\gamma = \sum_{l,r} \sum_{l',r'} c_{l,r} O_{l,l'}^L O_{r,r'}^R c_{l',r'}$ , with  $|\Psi\rangle = c_{l,r} |l\rangle |r\rangle$ , can be computed in two step. (1)  $X_{r,r'} = \sum_l \sum_{l'} c_{l,r} O_{l,l'}^L c_{l',r'}$ . (2)  $\gamma = \sum_{r,r'} X_{r,r'} O_{r,r'}^R$ . The reason for contracting wave function with  $O^L$  first is that the dimension of  $O^L$  is  $4M$  while the dimension of  $O^R$  is  $M$ . The number of operation required for forming  $X$  is  $O(k^{N+1} M^3)$  and that for dot product between  $X$  and  $O^R$  is  $O(k^{2N} M^2)$ . The computations for N-RDM are  $O(k^{N+1} M^3 + k^{2N} M^2)$ .

With above process, an expectation value like  $\langle \hat{a}_0^\dagger \hat{a}_1^\dagger \hat{a}_2 \hat{a}_3 \rangle$  is obtained. For a non-spinadapted DMRG algorithm ( the operators in not a spin tensor), we can get the value of  $\gamma_{0,1,3,2}$  by permuting  $\hat{a}_2$  and  $\hat{a}_3$ . For spinadapted DMRG operators, what we get is a set of  $\langle \hat{a}_0^\dagger \hat{a}_1^\dagger \hat{a}_2 \hat{a}_3 \rangle$  values. They are  $\langle \{[(\hat{a}_0^\dagger \hat{a}_1^\dagger)_{\mathcal{S}}^{S_1} (\hat{a}_2)_{\mathcal{D}}]^{S_2} (\hat{a}_3)_{\mathcal{E}}\}^{S_3} \rangle$  with different spins  $S_1, S_2, S_3$ . The spin tensors can be expanded as linear combination of spin orbital operators and linear equations are formed for spin orbital RDM elements. With spin embedding, expectation values of all spin tensors with non-zero spin are zero, significantly decrease the number of expectation values to compute. The coefficients for these linear equations are the same for the operators in the same pattern and can be generated automatically and be reused. Computation cost for this process is not related the bond dimension,  $M$  and is ignorable compared to other parts.

The computation of 4RDM, which is needed in DMRG-NEVPT is  $O(k^8 M^2 + k^5 M^3)$ , much higher than that of DMRG optimization. Therefore, the bond dimension of MPS in 4RDM calculations is limited. With the same bond dimension, MPS from a “reverse schedule” sweep is usually better optimized than MPS from standard sweep schedule, in which the bond dimension is increased. All of our NEVPT calculations use MPS optimized through “reverse schedule”.

## II. CHROMIUM DIMER

Chromium dimer has been a challenging problem in quantum chemistry, because large active space is needed to simulate its potential energy curve correct. At the same time, dynamic correlation is also required for a qualitative potential energy curve.<sup>7,13,15,16,19,29-31</sup>

The CAS(12e,12o), derived from the 3d and 4s atomic orbitals, was widely employed for chromium

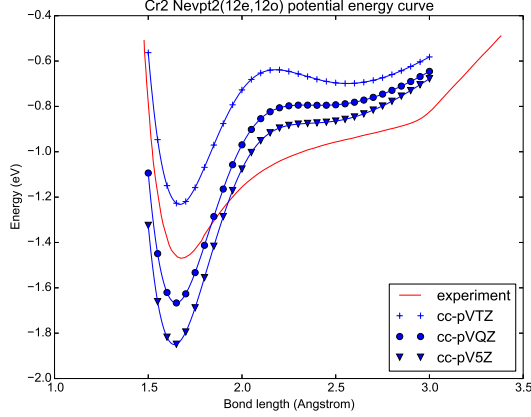


FIG. 1. NEVPT2(12e,12o) potential energy curve with a suite cc-pvxx basis set ( $x=t,q,5$ )

The Energy is relative to the isolated atoms.

dimer calculations.<sup>15,16,19,29–31</sup> Both CASPT2<sup>29–31</sup> and NEVPT2<sup>11</sup> based CASSCF(12e,12o) reference function overestimate the dissociation energy of the 3d-3d bond, especially when large basis sets, e.g. g-, h-, or even i- type function, were used.<sup>14,15</sup> And the results from CASPT2(12e,12o) are heavily sensitive to the choice of the zero-order Hamiltonian.<sup>14,17</sup> According to NEVPT3 study,<sup>15</sup> the common CAS(12e,12o) wave function is not a good starting reference for the perturbation theory, because the third-order perturbation results in a large fluctuation and an unreasonable curve. DMRG-CASPT2 calculation with a CAS(12e,28o), derived from 3d, 4s, 4p, 4d atomic orbitals, gave potential energy curves close to the experimental one. However, different zero-order Hamiltonians, due to different level shifts in CASPT2, gave quantitatively different results. The difference of  $D_e$  with different level shifts was about 0.2eV.<sup>7</sup> DMRG-NEVPT2 is free of intruder state and there is no need add “level shift” to change zero-order Hamiltonian. It should be feasible to describe chromium dimer potential energy curve.

A suite of cc-pvxx ( $x = t,q,5$ ) basis sets was used in our calculations. No basis set superposition error (BSSE) corrections were applied in the calculations because the BSSE was regarded as small for the large basis sets including h or i-type functions. Isolated atoms were used as energy reference, which was consistent with extremely long (30Å) dimer.

For the NEVPT2(12e,12o) potential energy curve of Cr<sub>2</sub> in II, larger basis set gives a deeper and, sometimes, worse, curve. It is agree with previous studies with atomic natural orbital (ANO) basis sets. Then the (12e,12o) CAS was extended by adding  $\{\sigma_g, \sigma_u, \pi_g, \pi_u, \pi'_g, \pi'_u\}$  orbitals, dominant components of which are 4p and 4d orbitals (after orbital optimization, mainly 4d orbitals), forming a (12e,18o) CAS. Due to exponential computation of FCI, DMRG becomes necessary. Before DMRG-NEVPT2 calculation, orbitals were

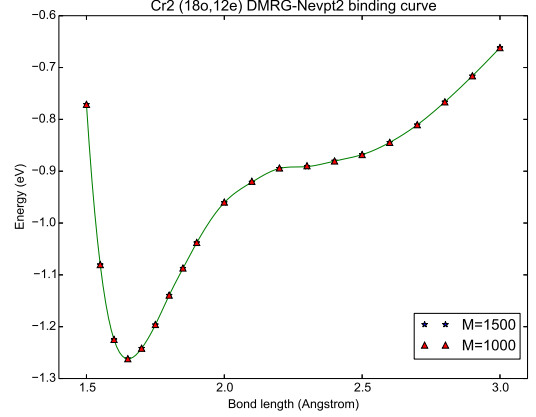


FIG. 2. DMRG-NEVPT2(12e,18o) results with different bond dimension

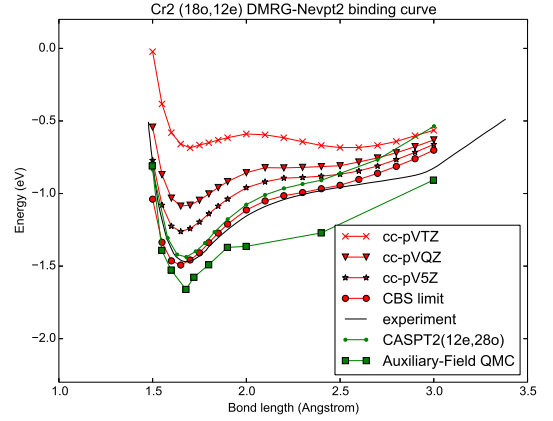


FIG. 3. DMRG-NEVPT2(12e,18o) potential energy curve with a suite cc-pvxx basis set ( $x=t,q,5$ ) and CBS limit

optimized with DMRG-SCF with  $M = 1000$ , through Pyscf and Block. There was no frozen core in the orbital optimization. Then reference MPS was optimized with  $M=4000$  and was then compressed into a MPS with  $M=1000$  through “reverse schedule”, with the optimized CAS. To check whether  $M$  is big enough, the potential energy curve with cc-pv5z basis was also calculated with  $M=1500$ . The difference between curving with  $M=1000$  and that with  $M=1500$  is ignorable.

Figure II shows the potential energy curve with a suite of cc-pvxx ( $x=t,q,5$ ) basis set and complete basis set (CBS) limit. A larger basis set still gives a deeper and better (not like CAS(12e,12o) result) curve.

Need logical reasons here. In the calculation described above, the relativistic effect was not included. And cc-

	$D_e(\text{eV})$	$R_0(\text{\AA})$	$\omega_e$
ccpv-xz CAS(12e,18o)	1.491	1.632	415
experiment	1.47(5)	1.679	480.6(5)

pvxz basis set might not be able to describe core-valence correlation well. The calculated potential energy curve was already quantitatively correct, compared to experimental one. However, there is definitely not enough evidence to say that relativistic effect is not important or that cc-pvpxz basis is enough for core-valence correlations. We used cc-pwcvxz-dk basis set and x2c Hamiltonian to get better accuracy.

At the same time, the 4d orbital were not fully included in the active space, only  $d_{z^2}, d_{xz}, d_{yz}$ .  $\delta$  bonds formed by  $d_{xy}$  and  $d_{x^2-y^2}$  were not included, because their orbital energies in mean-field and CASSCF (CAS(12e,12o)) calculations were higher than those of 4d  $\sigma$  and  $\pi$  orbitals. Including them in the active space would give a better result. However, the computations increased a lot. We had to decrease the bond dimension to 500 in DMRG-NEVPT2 calculation.

### III. POLY(P-PHENYLENE VINYLENE)

Poly(p-phenylene vinylene) is a type of phenyl-based light emitting conjugated polymers, which is useful for displays and photovoltaic devices. It has many low-lying states that participate in the photophysics and it was extensively investigated through theoretical methods, such as DMRG based on Pariser-Parr-Pople (PPP) model<sup>23,24</sup> and semi-empirical intermediate neglect of differential overlap (INDO) Hamiltonian with configuration interaction<sup>25</sup>. However, ab initio correlated wave function calculations were not often reported, because of the difficulty to include static and dynamic correlation together for a complex system. We used PPV-3 as an example and demonstrated how to predict the excitation energies for low-lying state through DMRG-NEVPT2 calculation and the accuracy of DMRG-NEVPT2 for conjugated polymer molecule.

In our calculations, we employed an active space of (22e, 22o) from the conjugated  $\pi$  orbitals. For the ground state  $S_0$ , we obtained the initial equilibrium geometry of PPV-3 via DMRG-CI geometry optimization, starting from a guess from DFT/B3LYP optimized geometry. The geometry optimization was first run at  $M = 1000$ , and then near the convergence at  $M = 2000$ . Canonical orbitals are used in the geometry optimization.

Then state-averaged calculations were performed for  $^1A_g$  (2 states) and  $B_u$  symmetry (3 states), with canonical orbitals of the ground state. To identify excited states, we computed the transition 1-RDM and transition 2-RDM from the ground state, and identified the state according to a dominant excitation signature. Based on the chosen active space,  $3^1B_u$  is identified as the first optically bright state, with a HOMO  $\rightarrow$  LUMO excitation signature. And  $2^2A_g$  in state-average calculation with 2 states ( $3^2A_g$  when more states were averaged) is the first dark state, with a HOMO-1  $\rightarrow$  LUMO + HOMO  $\rightarrow$  LUMO+1 and HOMO, HOMO  $\rightarrow$  LUMO, LUMO excitation signature. Due to lack of dynamic correlation ( $\sigma - \pi$

TABLE I. Excitation energy (eV) calculated from DMRG-NEVPT2 with canonical orbitals. States are labeled according to energies with  $M=750$ .

state	M=250	M=500	M=750	DMRG-CI(M=750)
$2^1A_g$	4.742	4.669	4.657	4.991
$1^1B_u$	4.027	4.191	4.180	5.269
$2^1B_u$	4.449	4.486	4.264	4.740
$3^1B_u$	5.090	4.328	4.600	5.132

TABLE II. Excitation energy (eV) calculated from DMRG-NEVPT2 with localized orbitals. States are labeled according to excitation signatures and energies with  $M=750$ .

state	M=500	M=750	DMRG-CI(M=750)
$1^1B_u$	3.8628	3.8625	5.1312
$2^1B_u$	4.4980	4.4978	4.4953
$2^1A_g$	4.6634	4.6634	4.8456
$3^1B_u$	4.8268	4.8262	4.7542
$4^1B_u$	4.8441	4.8443	4.7572

interaction), the energy order of excited states is significantly different with experimental results or calculations with PPP model.

After including dynamic correlation through DMRG-NEVPT2, the energy first bright state was much lowered and it became the first excited state ( $1^1B_u$ ). This is similar to low-lying excited states of polyenes, where dynamic correlations lower the ionic excited state ( $1^1B_u$ ) relative to covalent excited state ( $2^1A_g$ ). However, the energy order did not converge with the bond dimension in the calculation (Table I).

Localized orbitals usually give a better convergence for DMRG calculation.<sup>5</sup> Therefore, further DMRG-NEVPT2 calculations were carried out based on split-localized orbitals (localize the occupied and unoccupied  $\pi$  orbitals separately with Pipek-Mezey method<sup>32</sup>). The NEVPT2 energies were calculated for lowest 6 states (based on DMRG-CI energy). The excitation energies were converged into less than 0.6 meV with bond dimension (Table II). They were accurate enough to determine the energy order of low-lying excited states. The difference between calculated excitation energies from canonical orbital and those from local orbitals was big, and it might not be the same even when bond dimension is infinite. One reason is that the molecular geometry was optimized without symmetry restriction. Some integral terms, which should be zero according symmetry, were not exact zero. When local orbital orbitals were used, the symmetry restriction on the integral was removed.

The excitation energy of first bright state (3.86 eV) agrees well with results from other theoretical studies (3.88 eV<sup>25</sup>, 3.91 eV<sup>23</sup>). However, it deviated from the experimental value (3.5 eV<sup>33</sup>, 3.43 eV<sup>34</sup>) a lot. The reasons were that PPV oligomer was substituted with tertiary butyl end-group to become soluble in the experiment and that the solvent was not considered in the calculations.

## IV. CONCLUSION

In this work, we developed a general algorithm to compute different order RDMs for DMRG wave function, which can be used by many dynamic correlation methods. Through up to 4th order RDM, we combined DMRG and NEVPT2, a intruder state free second order multireference perturbation theory, to describe static and dynamic correlations at the same time, forming DMRG-NEVPT2 method. It made the calculations complex molecules with large active spaces possible.

To demonstrate the capability of DMRG-NEVPT2 method, we used this method to calculate the potential energy curve of chromium dimer and excited states of poly(p-phenylene vinylene). For chromium dimer, the extended active space included  $4d$  orbitals and the so called “double d” effect were considered. It gave quantitatively corrected potential energy curves, demonstrating that correlation from second shell orbitals were essential for chromium dimer. For light emitting conjugated polymers, Poly(p-phenylene vinylene), excitation energy of low-lying excited states were computed through DMRG-NEVPT2 with different orbitals in active space. The local orbitals calculation gave results converged with bond dimension much better than canonical orbitals. And the accuracy from local orbital DMRG-NEVPT2 is about  $0.6\text{meV}$ , relative to standard NEVPT2. While the environments were not included in the calculations, the energy order of excited states were reasonable.

Based on above two examples, DMRG-NEVPT2 is a intruder free perturbation methods and it can be used for the molecule where large active spaces are needed.

## V. ACKNOWLEDGEMENTS

<sup>1</sup>S. R. White, Physical Review Letters **69**, 2863 (1992).

<sup>2</sup>S. R. White, Physical Review B **48**, 10345 (1993).

<sup>3</sup>G. K.-L. Chan and M. Head-Gordon, The Journal of Chemical Physics **116**, 4462 (2002).

<sup>4</sup>S. Sharma, K. Sivalingam, F. Neese, and G. K.-L. Chan, Nature Chemistry **6**, 927 (2014).

<sup>5</sup>R. Olivares-Amaya, W. Hu, N. Nakatani, S. Sharma, J. Yang, and G. K.-L. Chan, The Journal of Chemical Physics **142**, 034102 (2015).

<sup>6</sup>J. Yang, W. Hu, D. Usvyat, D. Matthews, M. Schtz, and G. K.-L. Chan, Science **345**, 640 (2014).

<sup>7</sup>Y. Kurashige and T. Yanai, The Journal of Chemical Physics **135**, 094104 (2011).

<sup>8</sup>S. Sharma and G. K.-L. Chan, The Journal of Chemical Physics **141**, 111101 (2014).

<sup>9</sup>E. Neuscamman, T. Yanai, and G. K.-L. Chan, International Reviews in Physical Chemistry **29**, 231 (2010).

<sup>10</sup>C. Angeli, R. Cimiraglia, S. Evangelisti, T. Leininger, and J.-P. Malrieu, The Journal of Chemical Physics **114**, 10252 (2001).

<sup>11</sup>C. Angeli, R. Cimiraglia, and J.-P. Malrieu, Chemical Physics Letters **350**, 297 (2001).

<sup>12</sup>C. Angeli, R. Cimiraglia, and J.-P. Malrieu, The Journal of Chemical Physics **117**, 9138 (2002).

<sup>13</sup>B. O. Roos, Collection of Czechoslovak Chemical Communications **68**, 265 (2003).

<sup>14</sup>P. Celani, H. Stoll, H.-J. Werner, and P. J. K. \*, Molecular Physics **102**, 2369 (2004).

<sup>15</sup>C. Angeli, B. Bories, A. Cavallini, and R. Cimiraglia, The Journal of Chemical Physics **124**, 054108 (2006).

<sup>16</sup>T. Mller, The Journal of Physical Chemistry A **113**, 12729 (2009).

<sup>17</sup>F. Ruiperez, F. Aquilante, J. M. Ugalde, and I. Infante, Journal of Chemical Theory and Computation **7**, 1640 (2011).

<sup>18</sup>Y. Kurashige, Molecular Physics **112**, 1485 (2014).

<sup>19</sup>S. Sharma and A. Alavi, The Journal of Chemical Physics **143**, 102815 (2015).

<sup>20</sup>J. H. Burroughes, D. D. C. Bradley, A. R. Brown, R. N. Marks, K. Mackay, R. H. Friend, P. L. Burns, and A. B. Holmes, Nature **347**, 539 (1990).

<sup>21</sup>R. H. Friend, R. W. Gymer, A. B. Holmes, J. H. Burroughes, R. N. Marks, C. Taliani, D. D. C. Bradley, D. A. D. Santos, J. L. Brdas, M. Lgdlund, and W. R. Salaneck, Nature **397**, 121 (1999).

<sup>22</sup>S. J. Martin, D. D. C. Bradley, P. A. Lane, H. Mellor, and P. L. Burn, Physical Review B **59**, 15133 (1999).

<sup>23</sup>A. Shukla, Physical Review B **65**, 125204 (2002).

<sup>24</sup>R. J. Bursill and W. Barford, The Journal of Chemical Physics **130**, 234302 (2009).

<sup>25</sup>D. Beljonne, Z. Shuai, R. H. Friend, and J. L. Brdas, The Journal of Chemical Physics **102**, 2042 (1995).

<sup>26</sup>K. G. Dyall, The Journal of Chemical Physics **102**, 4909 (1995).

<sup>27</sup>D. Ghosh, J. Hachmann, T. Yanai, and G. K.-L. Chan, The Journal of Chemical Physics **128**, 144117 (2008).

<sup>28</sup>D. Zgid and M. Nooijen, The Journal of Chemical Physics **128**, 144116 (2008).

<sup>29</sup>K. Andersson, B. O. Roos, P. Malmqvist, and P. O. Widmark, Chemical Physics Letters **230**, 391 (1994).

<sup>30</sup>B. O. Roos and K. Andersson, Chemical Physics Letters **245**, 215 (1995).

<sup>31</sup>B. O. Roos, K. Andersson, M. P. Flscher, P.-. Malmqvist, L. Serrano-Andrs, K. Pierloot, and M. Merchn, in *Advances in Chemical Physics*, edited by I. Prigogine and S. A. Rice (John Wiley & Sons, Inc., 1996) pp. 219–331.

<sup>32</sup>J. Pipek and P. G. Mezey, The Journal of Chemical Physics **90**, 4916 (1989).

<sup>33</sup>H. S. Woo, O. Lhost, S. C. Graham, D. D. C. Bradley, R. H. Friend, C. Quattrocchi, J. L. Brdas, R. Schenk, and K. Mllen, Synthetic Metals **59**, 13 (1993).

<sup>34</sup>G. H. Gelinck, J. J. Piet, B. R. Wegewijs, K. Mllen, J. Wildeman, G. Hadziioannou, and J. M. Warman, Physical Review B **62**, 1489 (2000).